

# Beaconless Auto-Alignment for Single-Wavelength 5 Tbit/s Mode-Division Multiplexing Free-Space Optical Communications

Yiming Li<sup>1\*</sup>, Gil Fernandes<sup>2</sup>, David Benton<sup>1</sup>, Antonin Billaud<sup>3</sup>,  
Mohammed Patel<sup>1</sup>, Andrew Ellis<sup>1</sup>

<sup>1\*</sup>Aston Institute of Photonic Technologies, Aston University,  
Birmingham, B4 7ET, UK.

<sup>2</sup>Instituto de Telecomunicações, University of Aveiro, Aveiro, 3810-193,  
Portugal.

<sup>3</sup>Cailabs, 1 Rue Nicolas Joseph Cugnot, Rennes, 35000, France.

\*Corresponding author(s). E-mail(s): [liy70@aston.ac.uk](mailto:liy70@aston.ac.uk);

Contributing authors: [gfernandes@av.it.pt](mailto:gfernandes@av.it.pt); [d.benton@aston.ac.uk](mailto:d.benton@aston.ac.uk);  
[antonin@cailabs.com](mailto:antonin@cailabs.com); [m.patel70@aston.ac.uk](mailto:m.patel70@aston.ac.uk); [andrew.ellis@aston.ac.uk](mailto:andrew.ellis@aston.ac.uk);

## Abstract

Mode-division multiplexing has shown its ability to significantly increase the capacity of free-space optical communications. An accurate alignment is crucial to enable such links due to possible performance degradation induced by mode crosstalk and narrow beam divergence. Conventionally, a beacon beam is necessary for system alignment due to multiple local maximums in the mode-division multiplexed beam profile. However, the beacon beam introduces excess system complexity, power consumption, and alignment errors. Here we demonstrate a beaconless system with significantly higher alignment accuracy and faster acquisition. This system also excludes excess complexity, power consumption, and alignment errors, facilitating simplified system calibration and supporting a record-high 5.14 Tbit/s line rate in a single-wavelength free-space optical link. We anticipate our paper to be a starting point for more sophisticated alignment scenarios in future multi-Terabit mode-division multiplexing free-space optical communications for long-distance applications with a generalised mode basis.

**Keywords:** Free-space optical communication, mode-division multiplexing, multiple-input multiple-output, alignment

# 1 Introduction

Mode-division multiplexing (MDM) is a promising technology to extend the capacity limits in free-space optical (FSO) communication systems [1]. Orthogonal to other degrees of freedom such as amplitude [2], phase [3], polarisation [4] and wavelength [5], MDM offers the spatial degree of freedom for multiplexing, extending capacity beyond the conventional limit in both FSO and fibre communications [1, 6]. Beyond conventional employment of orbital angular momentum (OAM) modes [1], which constitute an incomplete basis, there is a growing interest in employing complete mode basis, such as Hermite-Gaussian (HG) or Laguerre-Gaussian (LG) modes [7, 8], to maximise potential capacity gains in the spatial domain [9].

In contrast to fibre communications, FSO communication systems require stringent alignment to maximise received power [10]. In MDM systems, there is an additional requirement to minimise inter-mode crosstalk [11], thus increasing the demand for precise alignment systems. Although single-input single-output (SISO) FSO systems can naturally reuse the signal beam for alignment [10], most MDM FSO systems employed a beacon beam for alignment due to multiple local power extremums during the alignment [11, 12]. Although adaptive optics can be employed for alignment through tip/tilt compensation, it is also incompatible with generalised MDM systems due to the presence of multiple power extremums, and a beacon beam is still required [13]. While attempts have been made on beaconless alignment in OAM systems [14], it can not support complete mode bases such as HG or LG modes because certain modes have zero power on the x- and y-axis. Moreover, the employed quadrant-detector-based alignment structure still introduced practical alignment errors between the quadrant detector and the signal photodiodes. The errors were mitigated by introducing order intervals, which significantly reduced the number of applicable modes.

To minimise the inter-mode crosstalk in MDM system, it is important to reduce the practical optical calibration error between the signal and beacon beams, as well as between the quadrant detector and the signal photodiodes. Therefore, we should eliminate any excessive FSO paths, including the beacon beam and the 4-quadrant detector. This will also reduce the system cost and the difficulties in FSO calibration.

In this work, we demonstrate a beaconless and quadrant-detector-free alignment algorithm for HG-mode-based MDM system. By minimising power leakage to unwanted modes, this algorithm enables precise alignment to reduce inter-mode crosstalk. By eliminating redundant structures in alignment systems, it also reduces the overall cost of MDM FSO systems. When employing 6 lowest-order modes, this algorithm supported a  $6 \text{ (modes)} \times 2 \text{ (polarisations)} \times 80 \text{ GBaud}$  16-QAM transmission, obtaining a record-high line rate of 3.84 Tbit/s in single-wavelength FSO communication systems with a bit error rate (BER) below the hard-decision forward error correction (HD-FEC) limit. By employing probabilistic shaping (PS) 256-QAM in the same system, we achieved a record-high generalized mutual information (GMI) of 5.14 Tbit/s in single-wavelength FSO communication systems.

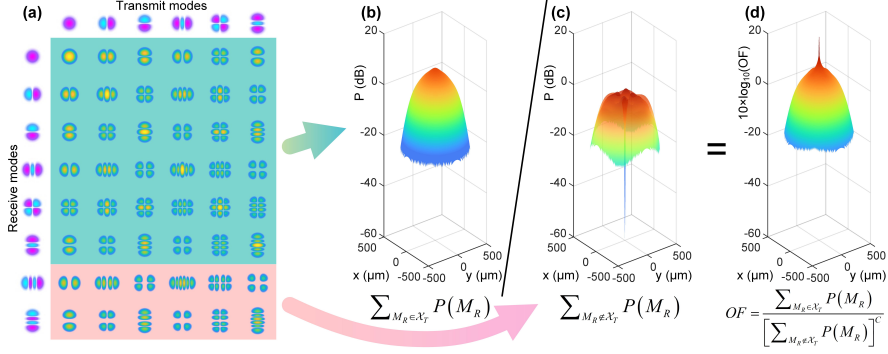


**Fig. 1** Concept of beaconless alignment. OF: objective function. (a) The scanning profile matrix from transmit HG modes to receive HG modes. (b) The received power summation of all transmitted modes at the receiver. (c) The received power summation of unwanted modes at the receiver. (d) The objective function.

## 2 Results

### 2.1 Hermite-Gaussian modes and the local maximums

As an orthogonal complete set to decompose a coherent paraxial beam, the electric field of the HG laser modes which propagate along the  $z$ -axis, can be described as [15]

$$E_{l,m}(x,y,z) = C_{l,m}^{HG} \frac{1}{w_z} \exp\left(-\frac{x^2+y^2}{w_z^2}\right) \exp\left[-\frac{ik(x^2+y^2)}{2R_z}\right] \times H_l\left(\frac{\sqrt{2}x}{w_z}\right) H_m\left(\frac{\sqrt{2}y}{w_z}\right) \exp(-i\psi_z) \exp(-ikz), \quad (1)$$

where  $C_{l,m}^{HG} = (2^{l+m-1}\pi!m!)^{-1/2}$  is the normalisation factor,  $R_z = (z_R^2 + z^2)/z$  is the radius of curvature,  $z_R = \pi w_0^2 n/\lambda$  is the Rayleigh range,  $w_0$  is the radius of beam waist,  $n$  is the refractive index,  $\lambda$  is the wavelength,  $w_z = w_0 \sqrt{1 + (z/z_R)^2}$  is the beam radius at  $z$ ,  $k = 2\pi/\lambda$  is the wave number,  $\psi_z = (l+m+1) \arctan(z/z_R)$  is the Gouy phase,  $H_n(x) = (-1)^n \exp(x^2) \frac{d^n}{dx^n} \exp(-x^2)$  is the Hermite polynomial of order  $n$ .

To calculate the received power from the transmitted mode  $M_t = HG_{l_t, m_t}$  to the received mode  $M_r = HG_{l_r, m_r}$ , the equation below applies:

$$P_{M_t, M_r} = \left( \iint E_{l_t, m_t}^*(x - \Delta x, y - \Delta y, z) E_{l_r, m_r}(x, y, z) dx dy \right)^2, \quad (2)$$

where  $(\Delta x, \Delta y)$  is the misalignment of the transmitted beam profile. As shown in Fig. 1(a), multiple local minimums occur when either the transmitted or the received mode is not  $HG_{0,0}$ , requesting the conventional beacon of an  $HG_{0,0}$  (Gaussian) beam.

## 2.2 Beaconless alignment

To align the MDM beam without a beacon, we need to find an objective function with only one local maximum where the system is optimally aligned.

### 2.2.1 The requirement of transmit modes

Intuitively, the overall power leakage to unwanted modes will increase when the misalignment is larger [16]. Although multiple local maximums exist in Fig. 1(a), the power summation of all transmitted modes is a suitable objective function with only one local maximum (Fig. 1(b)), which can be written as:

$$P_{Tx} = \sum_{M_r \in \mathcal{X}_T} P(M_r), \quad (3)$$

where  $\mathcal{X}_T$  is the set of all transmitted modes,  $P(M_r) = \sum_{M_t \in \mathcal{X}_T} P_{M_t, M_r}$  is the overall received power at receive mode  $M_r$ . Note the independence between the x- and y-axis indicated by Eq. (1), we can set  $y = 0$  and analyse the power distribution in the x-axis without loss of generality. As shown in Fig. 3(a), Eq. (3) works for all the tested situations from a total of 1 ( $HG_{0,0}$ ) to 20 ( $HG_{0,0} \sim HG_{19,0}$ ) transmitted modes. It is also worth noting that if  $HG_{L,M}$  is chosen as a transmitted mode, all  $HG_{l,m}$  modes that satisfy conditions  $0 \leq l \leq L$  and  $0 \leq m \leq M$  should also be chosen as transmitted modes to guarantee one single local maximum in Eq. (3).

Although the transmit HG modes form an orthogonal basis, their projections on the receive HG modes are not necessarily orthogonal to each other when misalignment exists. When unmodulated laser beams with inherent slow phase shifts are loaded into different transmit modes, the power collected by a specific receive mode will exhibit fluctuations. These fluctuations are due to the interference effect, which is influenced by the phase variations of different transmit modes. To eliminate this fluctuation in beaconless FSO systems, the phase of the laser source should be equally distributed in the time domain. This can be naturally achieved in coherent systems with phase modulation or quadrature amplitude modulation (QAM), or in direct detection systems with a slight modification to the intensity modulators to introduce a random phase shift of  $\pm\pi/2$ .

### 2.2.2 The requirement of receive modes

As shown in Fig. 3(a), the width of the “flat” top will increase when the number of modes increases, leading to a worse alignment accuracy when noise and practical imperfection exist. Therefore, a “sharp” metric is required when the system is nearly aligned. Exploiting the intrinsic orthogonality in HG modes, no power leakage to unwanted modes will be observed when the system is properly aligned (refer to the pink area in Fig. 1(a) for details). However, a small alignment error will introduce significant power leakage, especially to adjacent HG modes (e.g. from  $HG_{l,m-1}$  to  $HG_{l,m}$  in Fig. 1(a)). As shown in Fig. 1(c), when the system is properly aligned, a

sharp minimum can be observed in

$$P_{Rx} = \sum_{M_r \notin \mathcal{X}_T} P(M_r). \quad (4)$$

However,  $P_{Rx}$  will also reduce when the beam goes beyond the aperture, preventing Eq. (4) from being a stand-alone objective function. Fortunately, a higher mode order leads to a larger effective area. Therefore, dividing Eq. (3) by Eq. (4) will remove the problem of multiple local extremums when the misalignment goes to infinity. On the other hand, several local extremums are observed in Fig. 1(c) when the misalignment is a finite non-zero number. To eliminate these local extremums in the objective function, the monotonicity of Eq. (3) is exploited and a shaping coefficient  $C \leq 1$  is introduced in Eq. (5).

Given the x-axis misalignment insensitivity of the unwanted mode  $HG_{0,m+1}$  and y-axis misalignment insensitivity of the unwanted mode  $HG_{l+1,0}$ , it is suggested to incorporate at least two additional receive modes (e.g.  $HG_{0,m+1}$  and  $HG_{l+1,0}$ ) to improve alignment accuracy and obtain directional sensitivity, improving the acquisition speed in a quadrant-detector-free system. Moreover, including extra receive modes (e.g.  $HG_{0,m+2}$  and  $HG_{l+2,0}$ ) can further suppress practical errors and enhance the performance of the objective function. Importantly, it should be noted that in a quadrant-detector-free system, the directional sensitivity is unattainable in a Gaussian-beacon-based alignment system.

### 2.2.3 The objective function

As shown in Fig. 1(d), invoking Eq. (3) and Eq. (4), one suitable objective function can be written as

$$OF = \frac{P_{Tx}}{P_{Rx}^C} = \frac{\sum_{M_r \in \mathcal{X}_T} P(M_r)}{[\sum_{M_r \notin \mathcal{X}_T} P(M_r)]^C}, \quad (5)$$

where  $C \leq 1$  is a shaping coefficient. Multiple benefits can be obtained by employing the proposed objective function, including:

1. **Better alignment accuracy:** When the system is nearly aligned, utilising the power leakage to the unwanted modes (Eq. (4)) yields a 'sharp' metric (Fig. 1(d)) in the proposed objective function (Eq. (5)), thereby achieving significantly higher accuracy compared to conventional methods. By excluding the beacon beam, the practical error between the signal beam and the beacon beam is also eliminated.
2. **Faster acquisition:** The utilisation of transmitted higher-order modes (Eq. (3)) in the proposed objective function (Eq. (5)) allows a larger power profile (Fig. 3(a)). Without sacrificing alignment accuracy, a larger acquisition step can be employed to reduce the number of iterations for faster acquisition.
3. **Simplified system calibration:** The system calibration process is significantly simplified by excluding all the redundant optical structures such as beacon beam or 4-quadrant detector.
4. **Better cost and energy efficiency:** The proposed objective function can be achieved by employing simple photodiodes, typically integrated at the input of receiver erbium-doped fiber amplifiers (EDFAs) for amplification control. By

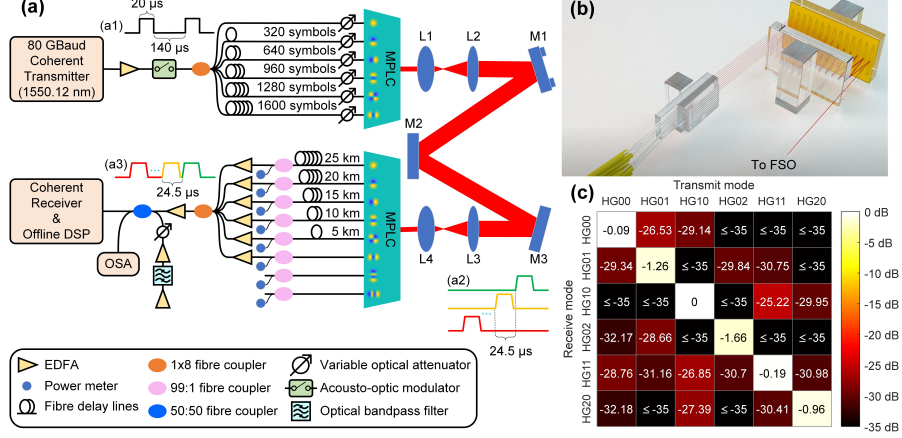


**Fig. 2** Experimental setup for beaconless MDM communication system. L: lens; M: mirror; EDFA: erbium-doped fiber amplifier; MPLC: multi-plane light conversion; OSA: optical spectrum analyser; FSO: free-space optics. (a) Schematic diagram of experimental setup. (b) The structure of the multi-plane light conversion (MPLC) device. (c) The normalised transfer matrix when the system is properly aligned.

excluding all the redundant optical structures, the system cost can be significantly reduced, with a higher energy efficiency by excluding power absorption on the redundant devices (e.g. wavelength beam splitters).

### 2.3 Experimental setup

Our experimental MDM multiple-input multiple-output (MIMO) FSO communication system is depicted in Fig. 2. At the transmitter, a 1550.12 nm laser was modulated by a dual-polarisation (DP) in-phase and quadrature (IQ) modulator with a nominal 6 dB bandwidth of 45 GHz using a 4-channel 120 GSa/s arbitrary waveform generator (AWG) with a 3 dB bandwidth of 50 GHz, and a 80 GBaud signal was generated. The signal was root-raised cosine (RRC) shaped with a roll-off factor of 0.1. The signal had a frame structure of 20,000 symbols with 1,920 quadrature phase-shift keying (QPSK) symbols in the training sequence, and 1 random QPSK pilot symbol for every 9 data symbols, the data symbols were either 16-QAM symbols generated from a  $2^{15} - 1$  pseudo random binary sequence (PRBS) or PS-256-QAM symbols generated from a mt19937ar Mersenne Twister [17]. After amplified by an EDFA, the signals were passed through an acousto-optic modulator (AOM) to generate a 20  $\mu$ s burst signal for each 160  $\mu$ s period (Fig. 2(a1)) to enable the time-division multiplexing (TDM) receiver setup which will be detailed later. To emulate independent transmitters, 6 copies were split from the burst signal and delayed by variable fibre delay lines (FDLs) with lengths of 0, 320, 640, 960, 1280, and 1600 symbols. The delayed signals were passed through variable optical attenuators (VOAs) to compensate for practical power differences before the VOAs. The compensated signals were then converted to corresponding HG modes using MPLC technology (Fig. 2(b), the output beam waist diameter of  $HG_{0,0}$  mode is approximately 0.3 mm) [18].

In the FSO channel, the transmitted HG modes were passed through a beam expander consisting of a convex lens with a focal length of 30 mm (L1) followed by another convex lens with a focal length of 100 mm (L2). The expanded beam was passed through a steering mirror (M1) with two high-precision motorised actuators for automatic alignment. The stepper motors of the actuators support an incremental motion of approximately 1  $\mu\text{m}$  in standard mode or approximately 0.5 nm using micro-steps in high-precision mode, providing adequate precision for our experiments. The beam was then passed through two more mirrors (M2, M3), and another symmetric beam expander consisting of a convex lens with a focal length of 100 mm (L3) followed by another convex lens with a focal length of 30 mm (L4). The beam was then coupled into the receiver MPLC device after a total FSO length of  $\sim 1.6$  m. As shown in Fig. 2(c), the normalised transfer matrix can achieve  $< 1.7$  dB mode-dependent loss, and  $> 25$  dB suppression for  $6 \times 6$  MIMO when the system is properly aligned using the proposed algorithm.

At the receiver, the optical signals split by the receiver MPLC device were delayed by the FDLs for the 6 lowest order modes to realise the TDM receiver. Here, a 5 km difference between adjacent modes introduced a  $\sim 24.5$   $\mu\text{s}$  delay (Fig. 2(a2)), slightly longer than the signal burst (Fig. 2(a1)). Each delayed signal was then split by a 99:1 fibre coupler so that the overall power received by each mode could be measured by a corresponding power meter. Here, we also connected two more unused higher-order modes (i.e.  $HG_{0,3}$  and  $HG_{3,0}$ ) to calculate the denominator term in Eq. (5). The 6 lowest order modes were then amplified by 6 EDFAs, coupled into one single-mode fibre (SMF) for TDM combining (Fig. 2(a3)), and amplified by another EDFA. Afterwards, the variable optical noise was loaded by a sequence of devices involving an EDFA, an optical bandpass filter, another EDFA, a VOA, and a 50:50 coupler. The average optical signal-to-noise ratio (OSNR) was then accessed using an optical spectrum analyser (OSA) to facilitate OSNR scanning. Finally, the TDM signals were received by a coherent receiver with a 70 GHz, 200 GSa/s oscilloscope and demodulated by offline digital signal processing (DSP).

## 2.4 Experimental results on alignments

We transmitted the 6 lowest order modes and employed  $HG_{0,3}$  and  $HG_{3,0}$  as unwanted receive modes for better alignment accuracy. Equipped with the proposed objective function, we're ready to align the system by employing the greedy algorithm [19]. Our strategy was to sequentially move towards nine neighbouring points including  $(-\Delta x, -\Delta x)$ ,  $(-\Delta x, 0)$ ,  $(-\Delta x, \Delta x)$ ,  $(0, -\Delta x)$ ,  $(0, 0)$ ,  $(0, \Delta x)$ ,  $(\Delta x, -\Delta x)$ ,  $(\Delta x, 0)$ , and  $(\Delta x, \Delta x)$ , where  $\Delta x$  is the step size. We recorded the objective function for all nine points and specifically targeted the point with the maximum value of the objective function. Repeating the greedy algorithm ensures precise alignment by focusing on the most favourable point within the immediate vicinity. The alignment traces of a  $6 \times 8$  MDM system from different starting points are depicted in Fig. 3(b). A beam profile including 6 transmitted modes is also depicted in Fig. 3(b) as a reference. Here the HG modes are rotated by  $45^\circ$  for symmetric considerations when designing the MPLC device [18]. Despite the choice of different initialisation points, the system could always converge to the centre of the beam profile. Moreover, the alignment traces

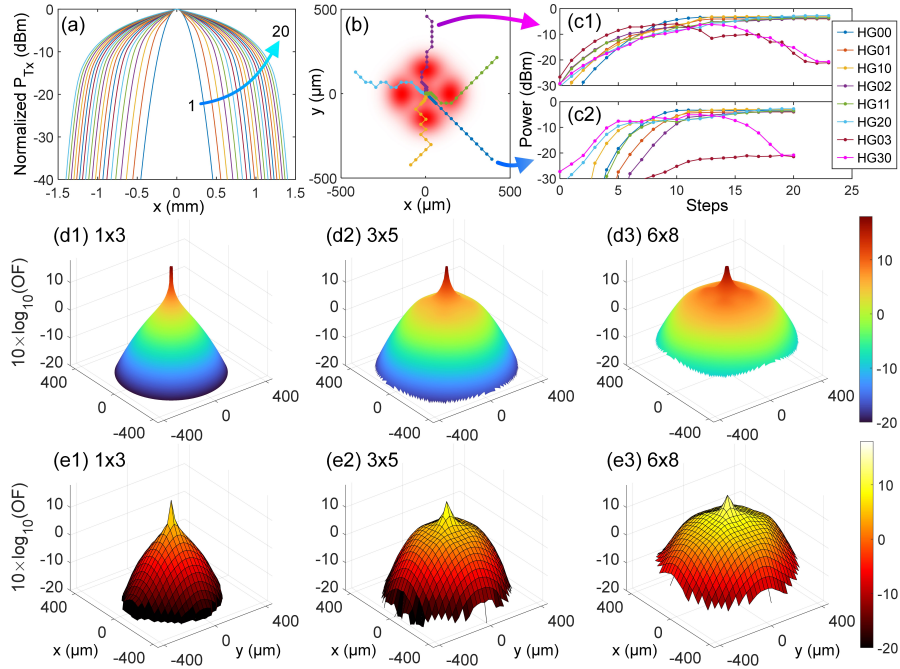


**Fig. 3** Summation of received power versus misalignment. (a) Received power profile versus x-axis misalignment. (b) Traces of alignments from different initial points. (c) Mode-wise received power versus alignment steps for the y-axis and diagonal misalignments, respectively. (d) Simulational objective function versus misalignment for  $1 \times 3$ ,  $3 \times 5$ , and  $6 \times 8$  systems, respectively. (e) Experimental objective function versus misalignment for  $1 \times 3$ ,  $3 \times 5$ , and  $6 \times 8$  systems, respectively.

tend to follow diagonal directions, which aligns with the “diagonal ridge” effect in the objective function as shown in Fig. 3(d3) and Fig. 3(e3).

The mode-wise received power of two typical alignment curves (along the y-axis and diagonal direction, respectively) is depicted in Fig. 3(c1)-(c2). As anticipated, the power of transmitted modes reached its maximum, while the power of unwanted modes was minimised when the system was properly aligned. After step 15, the unwanted modes made substantial contributions when the power of the transmitted mode reached a near-consistent level, indicating the importance of the “sharp” metric in the proposed objective function for precise alignment. Furthermore, the directional sensitivity between  $HG_{l,0}$  and  $HG_{0,m}$  is evident in Fig. 3(c2) when the path follows the same direction as  $HG_{l,0}$  modes.

By deliberately misaligning the system away from its aligned central point, we can compare the experimental objective function against the simulation results. As shown in Fig. 3(d1)-(d3), the objective function works for  $1 \times 3$ ,  $3 \times 5$ , and  $6 \times 8$  MIMO systems when the lowest order modes (i.e. smallest  $l+m$ ) were employed. The experimental results in Fig. 3(e1)-(e3) align well with the corresponding simulation predictions. Moreover, the symmetry in the experimental results also indicated the high precision of the proposed objective function.



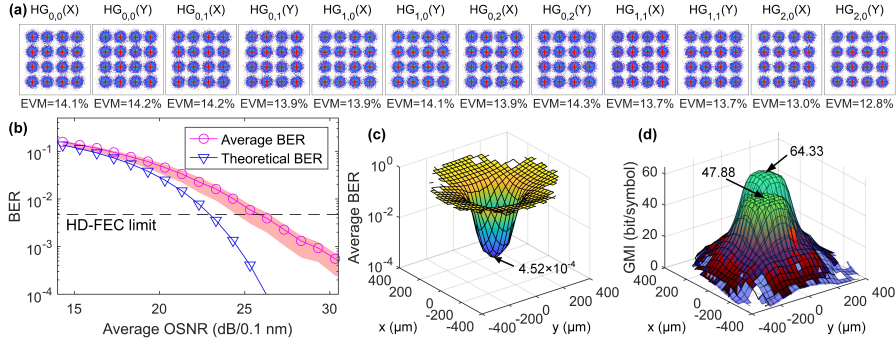


**Fig. 4** Experimental performance of communication system. EVM: error vector magnitude; BER: bit error rate; OSNR: optical signal-to-noise ratio; HD-FEC: hard-decision forward error correction; GMI: generalized mutual information. (a) Constellation diagram. (b) BER versus average OSNR. (c) BER versus misalignment. (d) GMI versus misalignment.

## 2.5 Achieved BER and data throughput

Fig. 4 shows the experimental performance of the proposed communication system, including the constellation diagram and the BER for 16-QAM signals, and the achievable data rate estimated from GMI for 16-QAM and PS-256-QAM signals, respectively. Fig. 4(a) depicts the channel-wise constellation diagrams for 16-QAM signals. Benefit from the proposed alignment algorithm, the constellations perform similarly in all channels, while some differences in error vector magnitude (EVM) are observed due to the mode-dependent loss introduced by the MPLC devices. Fig. 4(b) shows the mode-wise BER versus OSNR for 16-QAM signals. Here we observe an implementation penalty of approximately 2.9 dB from the theoretical limit at the HD-FEC limit of  $4.7 \times 10^{-3}$  [20]. This is mainly due to practical implementation loss including shot noise and quantisation noise introduced by the digital coherent receiver. As illustrated by the pink area, the channel-wise BER shows slight variations. Consistent with the EVM difference shown in Fig. 4(a), these variations are primarily attributed to the mode-dependent loss in the MPLC devices.

Fig. 4(c) depicts the BER performance versus the misalignment when the OSNR loading was disabled. When the system was properly aligned, we obtained a BER of  $4.52 \times 10^{-4}$ , an order of magnitude smaller than the HD-FEC limit. Moreover, an approximately 34% BER degradation was observed when the beam was deliberately misaligned by 30 μm, which was 1/10 of the  $HG_{0,0}$  beam diameter. Furthermore, the degradation significantly increased as the misalignment increased. This phenomenon indicated the importance of accurate alignment provided by our proposed algorithm. Fig. 4(d) depicts the GMI performance versus misalignment when the OSNR loading was disabled. The maximum GMI of 16-QAM signals are 47.88 bit/symbol, slightly smaller than the theoretical limit of 6 (modes) × 2 (polarisations) × 4 bit/symbol. By loading the PS-256-QAM signals, we obtained a maximum GMI of 64.33 bit/symbol, equivalent to an achievable line rate of 5.146 Tbit/s when transmitting 80 GBaud signals.

## 3 Methods

### 3.1 DSP details

A nonlinear Volterra predistorter was employed to compensate for the nonlinearities and imperfections in the 80 GBaud system [21, 22]. To perform the system identification, an 80 GBaud DP-16QAM probe signal with a roll-off factor of 0.1 was employed and a nonlinear filter with kernel memory lengths of (201,9,9) taps was created.

The offline DSP includes a sequential combination of the Gram-Schmidt orthogonalisation [23], polarisation demultiplexing in Stokes space [24], frequency-domain frequency offset estimation, frequency-domain chromatic dispersion (CD) compensation for the receiver FDLs [25], Godard timing recovery [26], phase-asynchronous phase and channel estimation [27], and 3-dimensional MIMO equalisation [28].

The shaping factor of PS-256-QAM is set to 2 to obtain  $<0.1$  dB signal-to-noise ratio (SNR) penalty when estimating data rate from GMI for up to 6 bit/symbol for the QAM constellations [29].

### 3.2 Measurement of transfer matrix

The normalised transfer matrix given in Fig. 2(c) was measured by sequentially connecting each mode of the transmitter MPLC directly to the transmitted signal which was amplified to 10 dBm by an EDFA. The power attenuation introduced by receiver FDLs were compensated to reflect proper power readings directly after the receiver MPLC. The power measurement of  $\leq -35$  dBm in Fig. 2(c) was due to the limited sensitivity of the power meters.

## 4 Discussion

We proposed a novel objective function for beaconless and quadrant-detector-free MDM FSO auto-alignment. This method significantly improved the alignment accuracy and acquisition speed. It also eliminated redundant hardware, reducing system cost, improving energy efficiency and facilitating system calibration. Moreover, this method supports a complete modal basis of Hermite-Gaussian modes. With identical beam divergence, this will enable the transmission of a significantly larger number of spatial channels compared to the incomplete OAM mode basis.

Our MDM FSO communication experiments demonstrated that the proposed alignment algorithm enables an inter-mode crosstalk suppression of  $>25$  dB in our  $6 \times 6$  MDM FSO communication system. By employing Volterra-based system identification, we achieved a record-high 80 GBaud in MDM transmissions, supporting up to a record-high 3.84 Tbit/s and 5.14 Tbit/s line rate when employing 16-QAM and PS-256-QAM signals, respectively.

Our proposed algorithm has shown superb alignment accuracy, inter-mode crosstalk suppression, and hardware efficiency. By exploiting spatial diversity, our experimental demonstration underpins the potential of ultra-high data rate MDM transmission. We anticipate this paper to be a starting point for more sophisticated

alignment scenarios in future MDM FSO communications for long-distance applications with generalised mode basis such as LG modes, Ince-Gaussian modes, Bessel modes, etc.

**Acknowledgements.** We acknowledge the support by EPSRC under Grants EP/T009047/1, EP/S003436/1, and EP/S016171/1, and by the European Union’s Horizon 2020 research and innovation programme under the Marie Skłodowska-Curie Grant 713694.

**Author contributions.** Y.L. and G.F. designed and carried out the experiment and analysed the data. A.B. designed and assembled the multi-plane light conversion devices. Y.L. and D.B. designed and calibrated the optical system. Y.L. designed and calibrated the DSP. M.P. and A.E. provided the technical support. Y.L. drafted the manuscript with support from all co-authors. A.E. supervised the project.

**Competing interests.** The authors declare no competing interests.

## References

- [1] Wang, J., Yang, J.-Y., Fazal, I.M., Ahmed, N., Yan, Y., Huang, H., Ren, Y., Yue, Y., Dolinar, S., Tur, M., *et al.*: Terabit free-space data transmission employing orbital angular momentum multiplexing. *Nature photonics* **6**(7), 488–496 (2012)
- [2] Ali, W., Cossu, G., Gilli, L., Ertunc, E., Messa, A., Sturmiolo, A., Ciaramella, E.: 10 Gbit/s OWC system for intra-data centers links. *IEEE Photonics Technology Letters* **31**(11), 805–808 (2019)
- [3] Lange, R., Smutny, B., Wandernoth, B., Czichy, R., Giggenbach, D.: 142 km, 5.625 Gbps free-space optical link based on homodyne BPSK modulation. In: *Free-space Laser Communication Technologies XVIII*, vol. 6105, pp. 68–76 (2006). SPIE
- [4] Bitachon, B.I., Horst, Y., Kulmer, L., Blatter, T., Keller, K., Bonnefois, A.M., Conan, J.-M., Lim, C., Montri, J., Perrault, P., *et al.*: Tbit/s single channel 53 km free-space optical transmission-assessing the feasibility of optical GEO-satellite feeder links. In: *European Conference and Exhibition on Optical Communication*, pp. 3–6 (2022). Optica Publishing Group
- [5] Ciaramella, E., Arimoto, Y., Contestabile, G., Presi, M., D’Errico, A., Guarino, V., Matsumoto, M.: 1.28 Terabit/s (32x40 Gbit/s) WDM transmission system for free space optical communications. *IEEE Journal on selected areas in communications* **27**(9), 1639–1645 (2009)
- [6] Rademacher, G., Puttnam, B.J., Luís, R.S., Eriksson, T.A., Fontaine, N.K., Mazur, M., Chen, H., Ryf, R., Neilson, D.T., Sillard, P., *et al.*: Peta-bit-per-second optical communications system using a standard cladding diameter 15-mode fiber. *Nature Communications* **12**(1), 4238 (2021)

- [7] Pang, K., Song, H., Zhao, Z., Zhang, R., Song, H., Xie, G., Li, L., Liu, C., Du, J., Molisch, A.F., *et al.*: 400-Gbit/s QPSK free-space optical communication link based on four-fold multiplexing of Hermite–Gaussian or Laguerre–Gaussian modes by varying both modal indices. *Optics letters* **43**(16), 3889–3892 (2018)
- [8] Li, Y., Chen, Z., Hu, Z., Benton, D.M., Ali, A.A., Patel, M., Lavery, M.P., Ellis, A.D.: Enhanced atmospheric turbulence resiliency with successive interference cancellation DSP in mode division multiplexing free-space optical links. *Journal of Lightwave Technology* **40**(24), 7769–7778 (2022)
- [9] Zhao, N., Li, X., Li, G., Kahn, J.M.: Capacity limits of spatially multiplexed free-space communication. *Nature photonics* **9**(12), 822–826 (2015)
- [10] Fernandes, M.A., Monteiro, P.P., Guiomar, F.P.: Free-space terabit optical interconnects. *Journal of Lightwave Technology* **40**(5), 1519–1526 (2022)
- [11] Abadi, M.M., Cox, M.A., Alsaigh, R.E., Viola, S., Forbes, A., Lavery, M.P.: A space division multiplexed free-space-optical communication system that can auto-locate and fully self align with a remote transceiver. *Scientific reports* **9**(1), 19687 (2019)
- [12] Li, L., Zhang, R., Zhao, Z., Xie, G., Liao, P., Pang, K., Song, H., Liu, C., Ren, Y., Labroille, G., *et al.*: High-capacity free-space optical communications between a ground transmitter and a ground receiver via a UAV using multiplexing of multiple orbital-angular-momentum beams. *Scientific reports* **7**(1), 17427 (2017)
- [13] Ren, Y., Xie, G., Huang, H., Ahmed, N., Yan, Y., Li, L., Bao, C., Lavery, M.P., Tur, M., Neifeld, M.A., *et al.*: Adaptive-optics-based simultaneous pre-and post-turbulence compensation of multiple orbital-angular-momentum beams in a bidirectional free-space optical link. *Optica* **1**(6), 376–382 (2014)
- [14] Li, L., Zhang, R., Xie, G., Ren, Y., Zhao, Z., Wang, Z., Liu, C., Song, H., Pang, K., Bock, R., *et al.*: Experimental demonstration of beaconless beam displacement tracking for an orbital angular momentum multiplexed free-space optical link. *Optics Letters* **43**(10), 2392–2395 (2018)
- [15] Beijersbergen, M.W., Allen, L., Veen, H., Woerdman, J.: Astigmatic laser mode converters and transfer of orbital angular momentum. *Optics Communications* **96**, 123–132 (1993) [https://doi.org/10.1016/0030-4018\(93\)90535-D](https://doi.org/10.1016/0030-4018(93)90535-D)
- [16] Benton, D., Li, Y., Billaud, A., Ellis, A.: Spatial mode division multiplexing of free-space optical communications using a pair of multiplane light converters and a micromirror array for turbulence emulation. In: *Photonics*, vol. 11, p. 241 (2024). MDPI
- [17] Matsumoto, M., Nishimura, T.: Mersenne twister: a 623-dimensionally equidistributed uniform pseudo-random number generator. *ACM Transactions on*

- Modeling and Computer Simulation (TOMACS) **8**(1), 3–30 (1998)
- [18] Fontaine, N.K., Ryf, R., Chen, H., Neilson, D.T., Kim, K., Carpenter, J.: Laguerre-Gaussian mode sorter. *Nature communications* **10**(1), 1865 (2019)
- [19] Fernandes, M.A., Brandão, B.T., Georgieva, P., Monteiro, P.P., Guiomar, F.P.: Adaptive optical beam alignment and link protection switching for 5G-over-FSO. *Optics Express* **29**(13), 20136–20149 (2021)
- [20] Alvarado, A., Agrell, E., Lavery, D., Maher, R., Bayvel, P.: Replacing the soft-decision FEC limit paradigm in the design of optical communication systems. *Journal of Lightwave Technology* **33**(20), 4338–4352 (2015)
- [21] Eun, C., Powers, E.J.: A new Volterra predistorter based on the indirect learning architecture. *IEEE transactions on signal processing* **45**(1), 223–227 (1997)
- [22] Nölle, M., Erkiñç, M.S., Emmerich, R., Schmidt-Langhorst, C., Elschner, R., Schubert, C.: Characterization and linearization of high bandwidth integrated optical transmitter modules. In: 2020 European Conference on Optical Communications (ECOC), pp. 1–4 (2020). IEEE
- [23] Fatadin, I., Savory, S.J., Ives, D.: Compensation of quadrature imbalance in an optical QPSK coherent receiver. *IEEE Photonics Technology Letters* **20**(20), 1733–1735 (2008)
- [24] Szafraniec, B., Nebendahl, B., Marshall, T.: Polarization demultiplexing in Stokes space. *Optics Express* **18**(17), 17928–17939 (2010)
- [25] Faruk, M.S., Savory, S.J.: Digital signal processing for coherent transceivers employing multilevel formats. *Journal of Lightwave Technology* **35**(5), 1125–1141 (2017)
- [26] Godard, D.: Passband timing recovery in an all-digital modem receiver. *IEEE Transactions on Communications* **26**(5), 517–523 (1978)
- [27] Li, Y., Chen, Z., Patel, M., Lavery, M.P., Ellis, A.D.: Phase and channel estimation for high-capacity phase-asynchronous mode-division multiplexing multiple-input multiple-output free-space optical communications in strong turbulent channels. *Journal of Lightwave Technology* (2024)
- [28] Randel, S., Ryf, R., Sierra, A., Winzer, P.J., Gnauck, A.H., Bolle, C.A., Essiambre, R.-J., Peckham, D.W., McCurdy, A., Lingle, R.:  $6 \times 56$ -Gb/s mode-division multiplexed transmission over 33-km few-mode fiber enabled by  $6 \times 6$  MIMO equalization. *Optics Express* **19**(17), 16697–16707 (2011)
- [29] Fehenberger, T., Alvarado, A., Böcherer, G., Hanik, N.: On probabilistic shaping of quadrature amplitude modulation for the nonlinear fiber channel. *Journal of*

